doi:10.3788/gzxb20144307.0723002

聚合物填充的狭缝波导定向耦合器的数值分析

郑传涛,黄小亮,罗倩倩,梁磊,张大明,王一丁
(吉林大学 电子科学与工程学院 集成光电子学国家重点联合实验室吉林大学实验区,长春 130012)

摘 要:利用亥姆霍兹方程和有限差分法,给出一种用于分析聚合物 SU-8 填充的双狭缝波导定向耦合特性的数值方法,推导出双耦合狭缝波导模式特性的特征方程,并做了离散化和稀疏化处理,得到耦合波导的模式场分布和有效折射率.通过求解最高阶偶对称和最高阶奇对称模式的有效折射率,得到 TE 和 TM 偏振态下定向耦合器的耦合长度.数值分析结果表明,当耦合间距小于 800 nm 时,耦合长度小于 100 μm.利用椭偏仪测得狭缝波导各层材料的光学参数随工作波长的色散关系,研究分析了双狭缝波导耦合长度和模式损耗的色散特性.分析显示,随着工作波长的增大,两种偏振模式下的耦合长度均减小,且 TM 模式下的耦合长度大于 TE 模式下的耦合长度,当工作波长为 1 550 nm 时,二者分别为 28.2 和 26.2 μm(两狭缝波导间的耦合间距为 0.5 μm 时).同时,模式损耗也随波长的增大而减小,且 TE 模式损耗大于 TM 模式损耗,当工作波长为 1 550 nm 时,TE 及 TM 模式的振幅衰减系数分别为 5.65 和 3.16 dB/cm.

关键词:导波光学; 定向耦合器; 狭缝波导; 聚合物
中图分类号:TN253 **文献标识码**:A **文章编号**:1004-4213(2014)07-0723002-7

Numerical Analysis on A Directional Coupler Formed by Two Polymer-filled Nanoscale Slot Waveguides

ZHENG Chuan-tao, HUANG Xiao-liang, LUO Qian-qian, LIANG Lei,
ZHANG Da-ming, WANG Yi-ding
(*State Key Laboratory on Integrated Optoelectronics, College of Electronic Science and Engineering, Jilin University, Changchun* 130012, *China*)

Abstract: In terms of Helmholtz equation and finite-difference time-domain method, a numerical approach for analyzing the directional coupling characteristics based on two SU-8 filled slot waveguides was proposed. The mode eigen equation of the coupling slot waveguides was derived and solved, and mode optical field distribution and effective refractive index were achieved. By using the effective refractive indices of the highest-order even symmetric mode and the highest-order odd symmetric modes, the coupling length under TE and TM polarizations was calculated. Numerical simulation results show that when the coupling gap is less than 800 nm, the coupling length is less than 100 μm. The wavelength dispersion characteristics of the used materials were measured with an ellipsoidmeter, and then the wavelength dispersion of coupling length and mode loss of the coupling slot waveguides were investigated. The analytical results reveal that the coupling length decreases as the wavelength increases under both polarizations, and under the same coupling gap, the coupling length under TM polarization is larger than that under TE polarization. The coupling lengths under TM and TE polarizations are 28.2 and 26.2 μm, respectively, when wavelength is 1 550 nm and coupling gap is 0.5 μm. In addition, the mode loss also decreases as wavelength increases, and the mode loss under TE polarization is larger than that under TM

Foundation item: The National Natural Science Foundation of China (Nos. 61107021, 61177027, 61077041 and 61001006), the Ministry of Education of China (Nos. 20110061120052 and 20120061130008), the China Postdoctoral Science Foundation funded project (Nos. 20110491299 and 2012T50297), the Science and Technology Department of Jilin Province of China (No. 20130522161JH), and the Special Funds of Basic Science and Technology of Jilin University (No. 201103076)

First author: ZHENG Chuan-Tao (1982—), male, associate professor, Ph. D. degree, mainly focuses on guided-wave optics and optoelectronics. Email: zhengchuantao@jlu.edu.cn

Received: Oct. 14, 2013; **Accepted**: Dec. 06, 2013

polarization. The loss coefficients under TE and TM polarizations are 5.65 and 3.16 dB/cm, respectively, when the wavelength is 1 550 nm.

Key words: Guided-wave optics; Directional coupler; Slot waveguide; Polymer

OCIS Codes: 230.7370; 230.3120;250.5460

0 Introduction

In 2004, Almeida *et al* firstly reported 2-D and 3-D slot waveguides [1]. Because of discontinuity of electric field along the interface between high-index layer and low-index layer, the optical field is well confined within the slot filled with low-index material. The formed optical field is 20 times larger than that of the traditional waveguide, such as polymer waveguide, Silicon-On-Insulator (SOI) waveguide and SiO_2/Si waveguide. Through applying electric field or doping amplifying materials within the slot region, high modulation efficiency and large amplifying gain can be obtained. So far, different devices based on slot waveguides including electro-optic switch[2], polarization splitter [3], four-wave mixer [4], waveguide sensor [5] were proposed.

Waveguide directional coupler can be adopted to form various optoelectronic devices, for example, the reported polymer directional coupler electro-optic switches [6-7], two-section reversed polymer directional coupler electro-optic switches [8-9], Y-fed polymer directional coupler electro-optic switch and modulator [10-11], etc. For the slot waveguide directional coupler, the coupling length is only tens of micrometers, and the device has smaller size compared with traditional directional coupler under a similar coupling gap. Previously, optical directional couplers based on two or three slot waveguides were analyzed by using rigorous full-vectorial analysis methods based on a finite-element scheme [12-13]. Ultra-compact polarization splitter [3] and cross-slot waveguide directional coupler [14] were experimentally demonstrated. However, the wavelength dispersion of a slot waveguide coupler fully considering wavelength dispersion of used materials are not reported, but it is urgently desired in Dense Wavelength Division Multiplexing (DWDM) optical systems.

SU-8 is an epoxy based photoresist for microelectronic optoelectronic and optic applications, and it has very high optical transparency above 360 nm. The film based on SU-8 with any form can be obtained using the normal simple processes, such as spin coat, soft bake, expose, Post Expose Bake (PEB) and develop, so SU-8 is suited for permanent applications where it is imaged, cured and left in place. Thus in this paper, in terms of Helmholtz equation and Finite-Difference Time-Domain (FDTD) method, a numerical approach for analyzing the effective refractive index and mode field distribution of a SU-8 filled slot waveguide directional coupler is proposed. The wavelength dispersion characteristics of coupling length and mode optical loss are discussed.

1 Structure and theory

1.1 Device structure

Fig. 1 depicts top-view and cross-section of a directional coupler based on two slot waveguides. The substrate material is silicon, the under cladding material is SiO_2, the high index material besides the slot region is silicon, and the material filled in the slot is SU-8 [15]. The silicon width and slot width are W_H and W_S, respectively, the coupling gap between the two waveguides is d, and the under cladding thickness, the slot thickness and the upper cladding thickness are h_1, h_2 and h_3, respectively. Under 1 550 nm wavelength, the refractive indices of silicon and silica are $n_1 = 3.48$ and $n_2 = 1.46$ [16], respectively, and their loss parameters can be neglected, that is, $\alpha_1 \approx 0$ and $\alpha_2 \approx 0$. Under 1 550 nm, the refractive index and bulk extinction coefficient of SU-8 measured by an ellipsoidmeter are $n_3 = 1.567\ 9$ and $\kappa_3 = 3.93\times10^{-5}$, respectively, and its bulk amplitude loss coefficient is

$$\alpha_3 = \left(\frac{2\pi}{\lambda_0}\right)\kappa_3 = 3.93\times10^{-5}\ \mathrm{m}^{-1} \tag{1}$$

As shown in Fig. 1(a), let the light input into waveguide 1, and after a propagation distance, the input light will fully output from waveguide 2. This distance is the coupling length of the slot waveguide coupler, denoted by L_c.

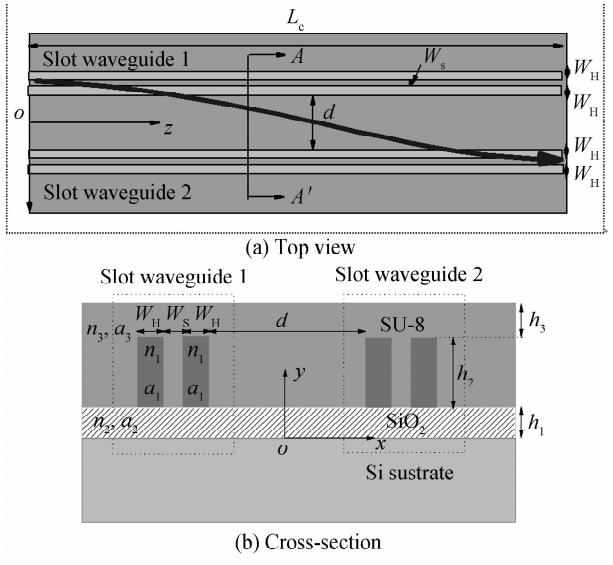

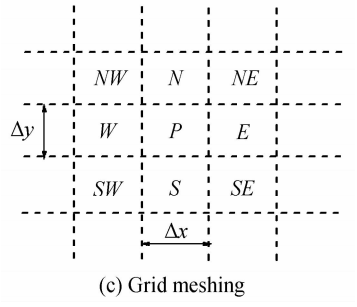

Fig. 1 Schematic diagram of the two directional coupling slot waveguides

1.2 Theory and formulation

To investigate the mode characteristics of two directional coupling slot waveguides, the full-wave vector eigen equation is given by [17]

$$\nabla^2 \boldsymbol{E} + \nabla\left[\frac{1}{n^2}\nabla(n^2)\cdot\boldsymbol{E}\right] + k^2 n^2 E = 0 \tag{2}$$

where k is wave number, n is refractive index distribution, and $\boldsymbol{E}$ is mode electric filed component. The electric field can be divided into two vectors, including $\boldsymbol{e}_t$ over the transverse direction and $\boldsymbol{e}_z$ over the propagation direction, that is

$$\boldsymbol{E}(x,y,z) = (\boldsymbol{e}_t + \boldsymbol{e}_z)\exp(-\mathrm{j}\beta z) \tag{3}$$

where β is propagation constant. Substituting Eq. (3) into Eq. (2), we obtain the full-wave vector eigen equation along the transverse direction

$$\nabla^2 \boldsymbol{e}_t + \nabla\left[\frac{1}{n^2}\nabla(n^2)\cdot\boldsymbol{e}_t\right] + k^2 n^2 \boldsymbol{e}_t = \beta^2 \boldsymbol{e}_t \tag{4}$$

The electric field along the propagation direction can be calculate by

$$\mathrm{j}\beta \boldsymbol{e}_z = \nabla\cdot\boldsymbol{e}_t + \frac{1}{n^2}\nabla(n^2)\cdot\boldsymbol{e}_t \tag{5}$$

Dividing $\boldsymbol{e}_t$ into horizontal component e_x and vertical component e_y, we can obtain from Eq. (3) that

$$\begin{bmatrix} P_{xx} & P_{xy} \\ P_{yx} & P_{yy} \end{bmatrix}\begin{bmatrix} e_x \\ e_y \end{bmatrix} = \beta^2 \begin{bmatrix} e_x \\ e_y \end{bmatrix} \tag{6}$$

where P_{xx}, P_{xy}, P_{yx} and P_{yy} are derivative coefficients. From Eq. (4), we have

$$\begin{aligned} P_{xx}e_x &= \frac{\partial}{\partial x}\left[\frac{1}{n^2}\frac{\partial(n^2 e_x)}{\partial x}\right] + \frac{\partial^2 e_x}{\partial y^2} + n^2 k^2 e_x \\ P_{yy}e_y &= \frac{\partial^2 e_y}{\partial x^2} + \frac{\partial}{\partial y}\left[\frac{1}{n^2}\frac{\partial(n^2 e_y)}{\partial y}\right] + n^2 k^2 e_y \\ P_{xy}e_y &= \frac{\partial}{\partial x}\left[\frac{1}{n^2}\frac{\partial n^2 e_y}{\partial y}\right] - \frac{\partial^2 e_y}{\partial x \partial y} \\ P_{yx}e_x &= \frac{\partial}{\partial y}\left[\frac{1}{n^2}\frac{\partial n^2 e_x}{\partial x}\right] - \frac{\partial^2 e_x}{\partial y \partial x} \end{aligned} \tag{7}$$

The mode field component along one direction is usually much smaller than that along another direction, therefore, in the following solution, only one component Φ is considered, which can be taken as e_x corresponding to TE polarization or e_y corresponding to TM polarization. For any Φ, when the refractive index is continuous, the characteristic equation given by Eq. (6) can be modified to

$$P\Phi(x,y) = \beta^2 \Phi(x,y) \tag{8}$$

where $P = \dfrac{\partial^2}{\partial x^2} + \dfrac{\partial^2}{\partial y^2} + n^2 k^2$. The cross-section shown in Fig. 1(a) is meshed, and the grid width and height along x and y direction are Δx and Δy, respectively. As shown in Fig. 1(b), when the refractive index distribution is discontinuous, the refractive indices and mode field components in grids P, W, E, N and S are n_P, n_W, n_E, n_N, n_S and Φ_P, Φ_W, Φ_E, Φ_N, Φ_S, and letting $\Phi(x,y) = \Phi_x(x) \times \Phi_y(y)$.

Take the field component e_x for analysis. Under certain x, at the boundaries of $y = \pm\Delta y/2$ (tangential direction), e_x is continuous. By using Lagrange interpolation function, $\Phi_y(y)$ in grids N, P and S possesses the same forms, which can be expressed as

$$\Phi_y(y) = A' + B'y + C'y^2 \tag{9}$$

Under certain y, at the boundaries of $x = \pm\Delta x/2$, e_x is discontinuous. By using Lagrange interpolation function, $\Phi_x(x)$ in grids W, P and E possesses different forms, which should be expressed as

$$\Phi_x(x) = \begin{cases} A'_W + B''x + C''x^2, & \text{cell } W \\ A'_P + B''x + C''x^2, & \text{cell } P \\ A'_E + B''x + C''x^2, & \text{cell } E \end{cases} \tag{10}$$

where A', B', C', A'_W, A'_P, A'_E, B'' and C' are expansion coefficients.

1) When $y=0$, $\Phi_y(y) = A'$. Let $A_W = A'_W A'$, $A_P = A'_P A'$, $A_E = A'_E A'$, $B = B''A'$ and $C = C''A'$. Then

$$\Phi(x,y) = \Phi(x) = \begin{cases} A_W + Bx + Cx^2, & \text{cell } W \\ A_P + Bx + Cx^2, & \text{cell } P \\ A_E + Bx + Cx^2, & \text{cell } E \end{cases} \tag{11}$$

Within the grid P, n^2 is a fixed value, then

$$\frac{\partial}{\partial x}\left[\frac{1}{n^2}\frac{\partial(n^2 e_x)}{\partial x}\right] = \frac{\partial^2 e_x}{\partial x^2} = 2C \tag{12}$$

At $x = \pm\Delta x/2$, $n^2 e_x$ is continuous, then we obtain

$$\begin{aligned} 2C = \frac{1}{(\Delta x)^2}\Bigg\{ & \frac{4(n_W^2 n_P^2 + n_E^2 n_W^2)}{n_P^4 + 2n_E^2 n_P^2 + 2n_W^2 n_P^2 + 3n_E^2 n_W^2} e_{xW} + \\ & \frac{4(n_E^2 n_P^2 + n_W^2 n_P^2 + 2n_E^2 n_W^2)}{n_P^4 + 2n_E^2 n_P^2 + 2n_W^2 n_P^2 + 3n_E^2 n_W^2} e_{xP} + \\ & \frac{4(n_E^2 n_P^2 + n_E^2 n_W^2)}{n_P^4 + 2n_E^2 n_P^2 + 2n_W^2 n_P^2 + 3n_E^2 n_W^2} e_{xE} \Bigg\} \end{aligned} \tag{13}$$

2) When $x=0$, $\Phi_x(x) = A'_P$, and then

$$\Phi(x,y) = A'_P A' + A'_P B' y + A'_P C' y^2 = A_P + B'''y + C'''y^2 \tag{14}$$

So

$$\partial^2 e_x/\partial y^2 = 2C''' \tag{15}$$

Considering that $e_{xP} = A_P$, $e_{xN} = A_P + B'''\Delta y + C'''\Delta y^2$ and $e_{xS} = A_P - B'''\Delta y + C'''\Delta y^2$, then

$$2C''' = \frac{1}{(\Delta y)^2}(e_{xN} + e_{xS} - 2e_{xP}) \tag{16}$$

Finally, for any central grid P, all parts of $P_{xx}e_x$

in Eq. (7) can be expressed as a linear equation using the electric field components in each grid. Combining all the grids within the whole waveguide cross-section, a matrix equation is achieved, and the coefficient matrix is a sparse matrix. The eigen values of the matrix are propagation constants of each mode, the corresponding vectors are mode field distribution, and they can be solved conveniently by MATLAB platform.

Define the effective refractive indices of the highest-order even symmetric mode and highest-order odd symmetric mode are $N_{\mathrm{ref,s}}$ and $N_{\mathrm{ref,a}}$, respectively. Therefore, the coupling length dependent on wavelength can be calculated by

$$L_{\mathrm{c}}(\lambda)=\frac{\lambda}{2[N_{\mathrm{ref,s}}(\lambda)-N_{\mathrm{ref,a}}(\lambda)]} \tag{17}$$

2 Single-mode design

Using the theory in Section 1, the mode characteristics of a single slot waveguide are analyzed for determining the waveguide size for fundamental mode propagation. The curve of effective refractive index of each mode versus the silicon width W_{H} is shown in Fig. 2, where the operation wavelength is 1 550 nm, W_{S} = 100 nm, h_1 = 475 nm, h_2 = 250 nm and h_3 = 475 nm. It can be seen that when W_{H} is taken as 200 nm, single mode propagation can be realized under both polarizations.

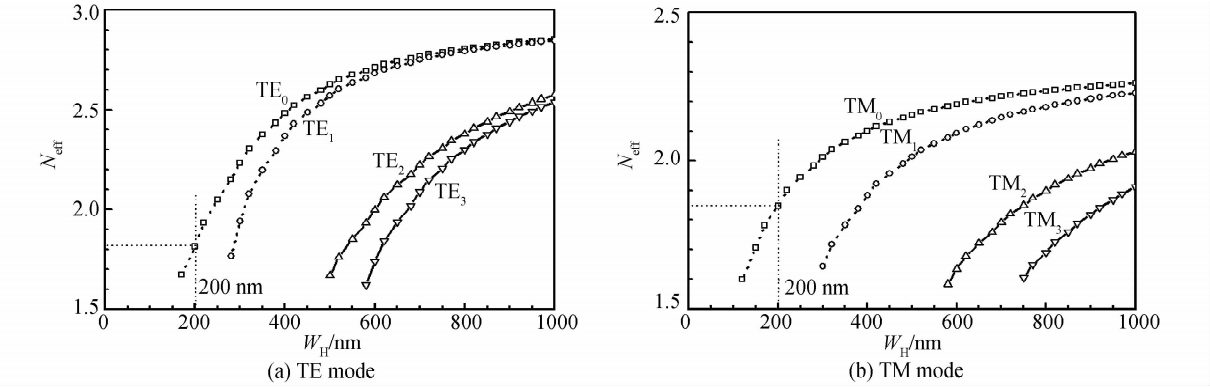

Fig. 2 For one single slot waveguide, curves of mode effective refractive indices versus silicon width W_{H}

3 Coupling characteristics

3.1 Even and odd mode distribution of the coupler

Under the single mode condition, for a pair of two directional coupling slot waveguides, the mode field distribution of the highest-order even symmetric mode and the highest-order odd symmetric mode are calculated and shown in Fig. 3, where the coupling gap is taken as d=500 nm.

3.2 Relation between coupling length and gap

Under 1 550 nm wavelength, for a pair of directional coupling slot waveguides, Fig. 4(a) reveals the curves of effective refractive indices of TE$_0$ (TM$_0$) mode and TE$_1$ (TM$_1$) mode versus the coupling gap between the two slot waveguides. It can be seen that, as the increase of coupling gap, $N_{\mathrm{ref,s}}$ decreases and $N_{\mathrm{ref,a}}$ increases, and they gradually approach to an identical value. By using Eq. (17), the relation between coupling length under TE polarization and coupling gap is shown in Fig. 4(b). When d is less than 800 nm, the coupling length L_{c} is less than 100 μm, which is obviously helpful for enhancing the device integrity. Similarly, $N_{\mathrm{ref,s}}$, $N_{\mathrm{ref,a}}$ and L_{c} under TM polarization are also calculated and exhibited in Fig. 5. From the comparison between Fig. 4 and Fig. 5, under

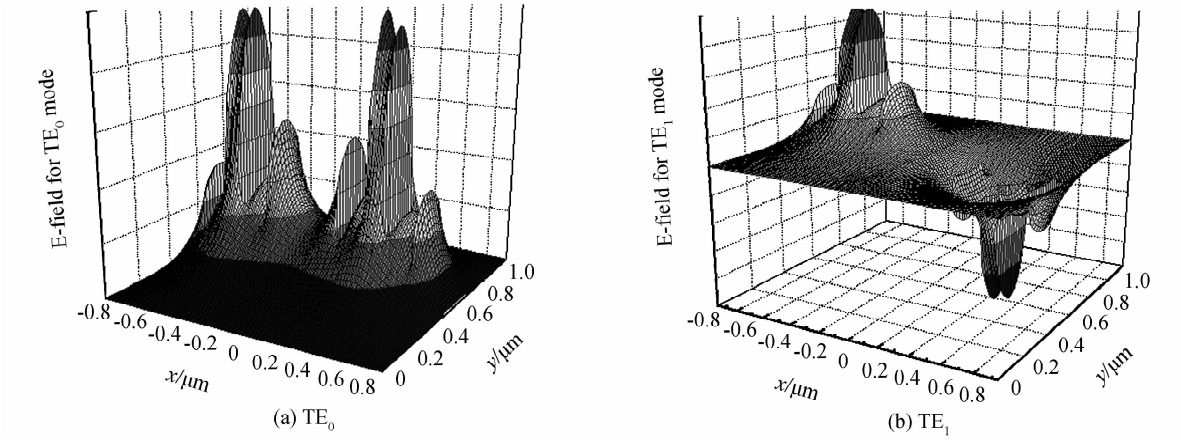

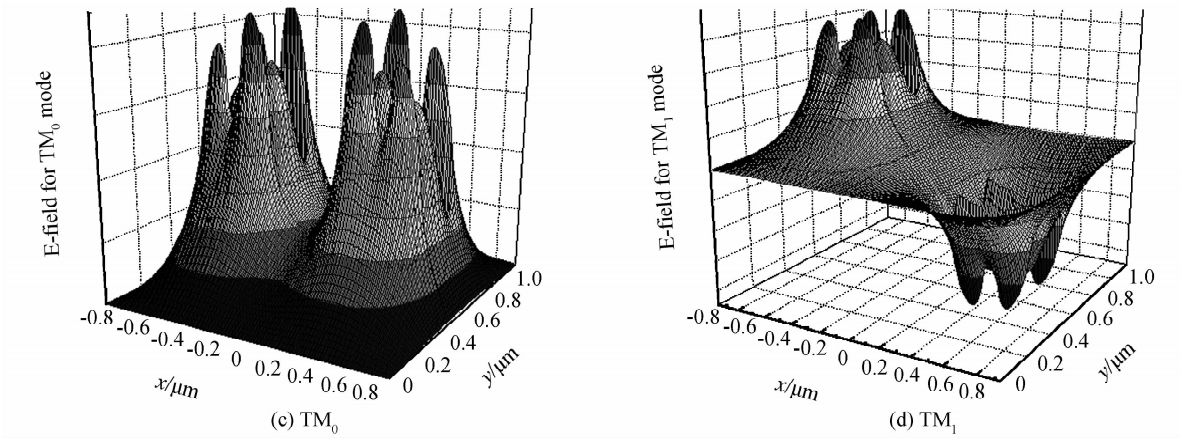

Fig. 3 Mode field distribution for a pair of directional coupling slot waveguides

the identical coupling gap, the coupling length under TM polarization is slightly larger than that under TE polarization. The variation of $N_{ref,s}$ and $N_{ref,a}$ versus d can be attributed below. When d is small, the coupling between the two slot waveguides is strong, and they can be treated as a single waveguide, where the highest order symmetric and asymmetric modes both exist. In each slot waveguide, the mode distribution is obviously different from its original distribution (for a single waveguide), leading to a large difference between $N_{ref,s}$ (or $N_{ref,a}$) and N_{eff} (for a single waveguide). When d gets larger, the coupling becomes weak. In each slot waveguide, the difference between the real mode distribution and its original distribution gets small, leading to a small difference between $N_{ref,s}$ (or $N_{ref,a}$) and N_{eff} (for a single waveguide). As d is extremely large, in each slot waveguide, the real mode distribution is actually its original distribution, e. g. $N_{ref,s} = N_{ref,a} = N_{eff}$. Under both polarizations, the relationships between $N_{ref,s}$, $N_{ref,a}$, L_c and d are obtained and shown by the fitting equations in Fig. 4 and Fig. 5.

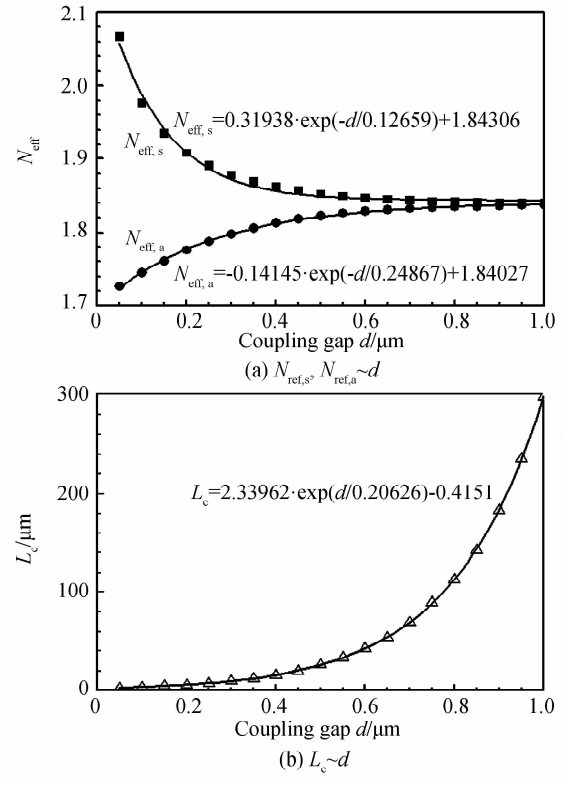

Fig. 4 Curves of $N_{ref,s}$, $N_{ref,a}$, and L_c versus d under TE polarization

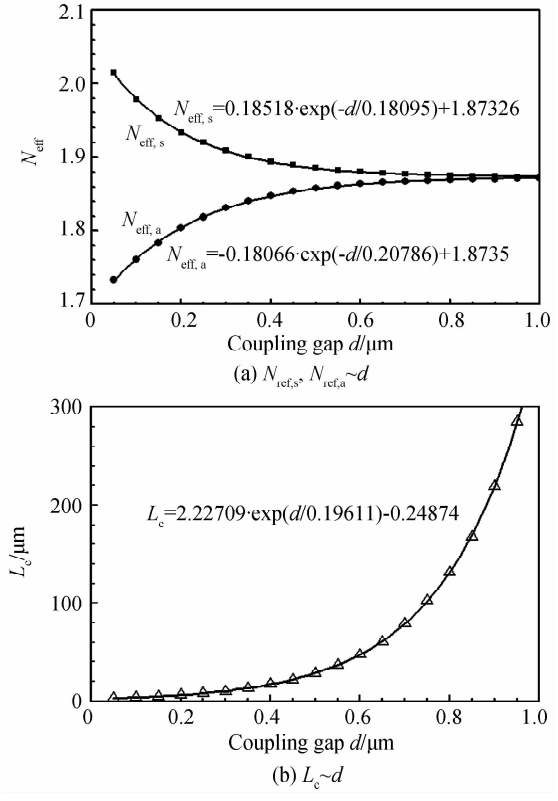

Fig. 5 Curves of $N_{ref,s}$, $N_{ref,a}$, and L_c versus d under TM polarization

3.3 Wavelength dispersion

To investigate the wavelength dispersion of the directional coupling slot waveguide, the refractive indices and extinction coefficient of Si, SiO_2 and SU-8 are measured by using an ellipsoidmeter and shown in Fig. 6. It can be observed that, the three refractive indices drop as wavelength increases. Considering these materials' wavelength dispersion, Fig. 7 shows the

curves of coupling lengths under the two polarizations versus the wavelength, where the coupling gap is taken as $d=0.5$ μm. We can see that L_c decreases with the increase of wavelength, and the coupling length under TM polarization is larger than that under TE polarization. The coupling lengths under the above two polarizations are 28.2 and 26.2 μm, respectively, under 1 550 nm wavelength and 0.5 μm coupling gap. Fig. 7 also shows relations between the fundamental mode amplitude loss coefficient and operation wavelength. The mode loss also decreases as wavelength increases, and the mode loss under TE polarization is larger than that under TM polarization. The loss coefficients under the above two polarizations are 5.65 and 3.16 dB/cm, respectively, under the operation wavelength of 1 550 nm.

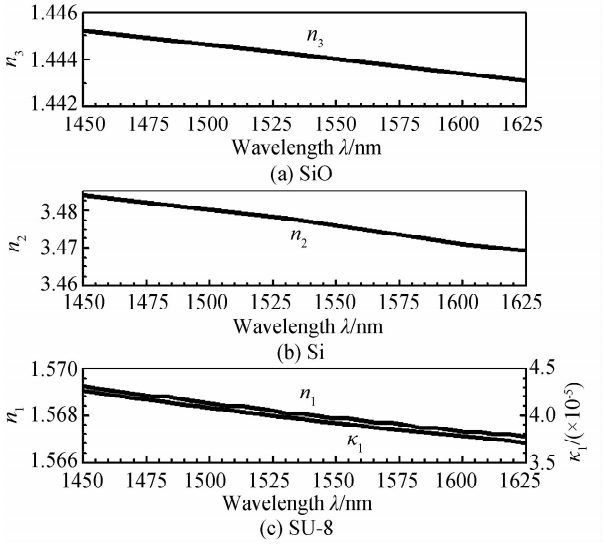

Fig. 6 Relations among refractive indices and extinction coefficient versus operation wavelength

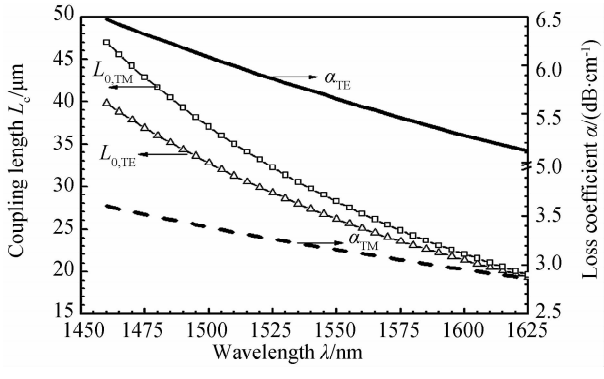

Fig. 7 Curves of coupling length and mode loss coefficient

3.4 Comparison and discussion

The proposed method is also used to calculate the coupling length of a GaAs cross-slot waveguide directional coupler operated at 1 580 and 1 540 nm wavelength under TE polarization [15]. The calculation results as well as the experimental results given in Ref. [14] are both listed in Table 1, where the center-to-center coupling gap is 880 nm. It can be found from Table 1 that the experimental results are in good agreement with the calculated results by the theory in this paper. This indicates that the proposed theory and related formulas proposed are reasonable in engineering design.

Table 1 Comparison between the calculated results using the proposed theory and the experimental results in Ref. [14]

Operation wavelength/nm		1 580	1 540
Coupling length under TE polarization /μm	The proposed theory	8.5	8.8
	Ref. [14]	8.4	9.0

Table 2 presents the calculated results on effective indices of TE and TM fundamental modes of slab slot waveguide using analytical method [1] and semivectorial numerical method based on FDTD, where the slot-width is 100 nm and the silicon width is 200 nm. It can be seen that the error is only −0.000 1 for TE mode, whereas that is about −0.001 7 for TM mode. Therefore, the proposed numerical method possesses acceptable accuracy and can meet the need of engineering design.

Table 2 Comparison between the calculated results using analytical method and semivectorial numerical method based on FDTD.

Method	Mode	Effective index	Error
TE	Analytical	2.949 4	−0.000 1
	numerical(this)	2.949 3	
TM	Analytical	2.324 6	−0.001 7
	numerical(this)	2.322 9	

4 Conclusion

In terms of Helmholtz equation and FDTD method, a numerical approach for analyzing the effective refractive index and mode field distribution of a directional coupler based on SU-8 filled slot waveguides is proposed. The wavelength dispersion of coupling length and mode optical loss are discussed. Numerical simulation shows that when the coupling gap is less than 800 nm, the coupling length is less than 100 μm, which will be helpful for enhancing device integrity and decreasing mode loss. The analysis results reveal that the coupling length decreases as the wavelength increases under both polarizations, and the coupling length under TM polarization is larger than that under TE polarization. The coupling lengths under the above two polarizations are 28.2 and 26.2 μm, respectively, when the wavelength is 1 550 nm and coupling gap is 0.5 μm. In addition, the mode loss also decreases as wavelength increases, and the mode loss under TE polarization is larger than that under TM

polarization. The loss coefficients under the above two states are 5.65 and 3.16 dB · cm^{-1}, respectively, under the operation wavelength of 1550 nm. The proposed analytical theory and results provide evidence for fabricating slot waveguide assisted devices, and are of practical reference values in engineering design.

References

[1] ALMEIDA V R, XU Q, BARRIOS C A, *et al*. Guiding and confining light in void nanostructure [J]. *Optical Letters*, 2004, **29**(11), 1209-1211.

[2] XIAO S M, WANG F, WANG X, *et al*. Electro-optic polymer assisted optical switch based on silicon slot structure [J]. *Optics Communications*, 2009, **282**(13): 2506-2510.

[3] LIN S, HU J, CROZIER K B. Ultracompact, broadband slot waveguide polarization splitter [J]. *Applied Physics Letters*, 2011, **98**(15), 151101.

[4] TRITA A, LACAVA C, MINZIONI P, *et al*. Ultra-high four wave mixing efficiency in slot waveguides with silicon nanocrystals [J]. *Applied Physics Letters*, 2011, **99**(19): 191105.

[5] LAI W, CHAKRAVARTY S, WANG X, *et al*. On-chip methane sensing by near-IR absorption signatures in a photonic crystal slot waveguide [J]. *Optical Letters*, 2011, **36**(6): 984-986.

[6] ZHENG C T, MA C S, YAN X, *et al*. Simulation and optimization of a polymer directional coupler electro-optic switch with push - pull electrodes [J]. *Optics Communications*, 2008, **281**(14): 3695-3702.

[7] ZHENG C T, MA C S, YAN X, *et al*. Analysis of response characteristics for polymer directional coupler electro-optic switches [J]. *Optics Communications*, 2008, **281**(24): 5998-6005.

[8] ZHENG C T, MA C S, YAN X, *et al*. Design of a polymer directional coupler electro-optic switch using two-section reversed electrodes [J]. *Applied Physics B*, 2009, **96**(1): 95-103.

[9] WANG R, ZHENG C T, SONG Q, *et al*. Fourier analysis of a polymer directional coupler electro-optic switch with two-section cosine-transitive CPWG electrodes: A new theoretical view [J]. *Optics Communications*, 2012, **285**(6): 1103-1112.

[10] ZHENG C T, MA C S, YAN X, *et al*. Design of integrated 1×2, 1×4 low driving voltage polymer electro-optic switches based on Y-fed directional couplers [J]. *Journal of Modern Optics*, 2009, **56**(5), 615-622.

[11] ZHENG C T, MA C S, YAN X, *et al*. Analysis and optimum design of a polymer Y-fed coupler electro-optic switch using double-section reversed electrodes [J]. *Journal of Modern Optics*, 2009, **56**(12), 1383-1391.

[12] FUJISAWA T, KOSHIBA M. Polarization-independent optical directional coupler based on slot waveguides [J]. *Optical Letters*, 2006, **31**(1): 56-58.

[13] XIAO J, LIU X L, SUN X. Design of polarization-independent optical couplers composed of three parallel slot waveguides [J]. *Applied Optics*, 2008, **47**(14), 2687-2695.

[14] TU X, ANG S S N, CHEW A B, *et al*. An ultracompact directional coupler based on GaAs cross-slot waveguide [J]. *IEEE Photonica Technology Letters*, 2010, **22**(17): 1324-1326.

[15] GAO L, SUN J, SUN X Q, *et al*. Low switching power 2×2 thermo-optic switch using direct ultraviolet photolithography process[J]. *Optics Communications*, 2009, **282**(20): 4091-4094.

[16] PALIK E. D. Handbook of optical constants of solids [M]. San Diego: Academic Press, 1985.

[17] 马春生, 刘式墉. 光波导模式理论 [M]. 长春: 吉林大学出版社, 2006.